



HAL
open science

A-amylose single crystals: influence of amylose concentration, crystallization temperature and surface induction on the crystal morphology

Nicole Montesanti, Christine Lancelon-Pin, Gabrielle Potocki-Veronese, Alain Buléon, Jean-Luc Putaux

► **To cite this version:**

Nicole Montesanti, Christine Lancelon-Pin, Gabrielle Potocki-Veronese, Alain Buléon, Jean-Luc Putaux. A-amylose single crystals: influence of amylose concentration, crystallization temperature and surface induction on the crystal morphology. *Cellulose*, 2023, 30 (13), pp.8459-8473. 10.1007/s10570-023-05387-2. hal-04195422

HAL Id: hal-04195422

<https://cnrs.hal.science/hal-04195422>

Submitted on 5 Sep 2023

HAL is a multi-disciplinary open access archive for the deposit and dissemination of scientific research documents, whether they are published or not. The documents may come from teaching and research institutions in France or abroad, or from public or private research centers.

L'archive ouverte pluridisciplinaire **HAL**, est destinée au dépôt et à la diffusion de documents scientifiques de niveau recherche, publiés ou non, émanant des établissements d'enseignement et de recherche français ou étrangers, des laboratoires publics ou privés.

A-amylose single crystals: influence of amylose concentration, crystallization temperature and surface induction on the crystal morphology

Nicole Montesanti^a, Christine Lancelon-Pin^a, Gabrielle Potocki-Veronese^b,
Alain Buléon^c, Jean-Luc Putaux^{a,*}

^a *Univ. Grenoble Alpes, CNRS, CERMAV, F-38000 Grenoble, France*

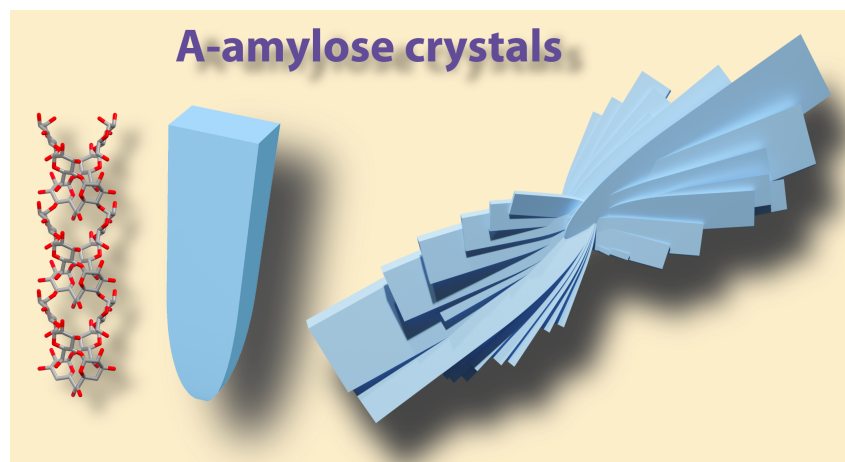
^b *TBI, CNRS, INRAE, INSAT, Université de Toulouse, F-31400 Toulouse, France*

^c *UR1268 Biopolymères Interactions Assemblages, INRAE, F-44316 Nantes, France*

*corresponding author: jean-luc.putaux@cermav.cnrs.fr

Published in: **Cellulose** 30 (2023), 8459-8473

<https://doi.org/10.1007/s10570-023-05387-2>



Abstract

Narrow fractions of short-chain enzymatically-synthesized amylose have been crystallized from 0.05-5.0% w/v aqueous solutions by slow diffusion of acetone or ethanol vapors at 50-60 °C or addition of hot liquid acetone. The fractions were selected according to their ability to form a few micrometer-long A-type acicular single crystals with a well-defined faceted habit. The single crystals grew organized into rosettes or fan-like assemblies whose relative fraction depended on the initial amylose concentration. Rosettes became dominant with increasing concentration while the aspect ratio of the constituting crystals increased with crystallization temperature. In rosettes, the density of crystals increased as well but without forming solid spherulites, due to the topological constraint of packing isomorphous platelet crystals growing from a common nucleus inside a spherical volume. A higher density of crystals was achieved by nucleation on the surface defects of inductive glass slides. Due to the chemical polarity of A-type amylose single crystals, rosettes and crystal mats exposed faces concentrating reducing amylose chain ends, available for chemical labelling or grafting.

Introduction

Amylose, one of the two main constituents of native starch granules, along with amylopectin, is a mostly linear homopolymer of D-glucopyranosyl units connected by $\alpha(1,4)$ bonds with less than 1% $\alpha(1,6)$ branching linkages (Pérez and Bertoft 2010). Amylose-like linear polymers can also be biosynthesized *in vitro* by amylose synthases such as α -glucanphosphorylase (Ohdan et al. 2006) or amylosucrases (Potocki de Montalk et al. 2000). While amylose is considered to play a minor role in the overall semicrystallinity of starch granules, it can be readily crystallized *in vitro*. The resulting morphology (gels, spherulites, crystals, etc.) and allomorphic type (so-called A and B) depend on the molecular weight, branching degree, and concentration of amylose, as well as on the type of solvent/precipitant and crystallization temperature (Gidley 1987, Buléon et al. 2007). Typically, A-amylose crystallizes in the presence of ethanol or acetone at 50–60 °C, while B-amylose forms in pure water at low temperature (Ring et al. 1987, Whittam et al. 1990). Allomorphs A and B have monoclinic and hexagonal unit cells, respectively, and consist of 6-fold left-handed double helices packed in a parallel fashion and associated with a number of water molecules (Buléon et al. 2007).

A-amylose crystallizes *in vitro* in the form of spindle-like crystals whose shape, size, and organization depend on the chain length, branching degree, polydispersity, and type of precipitant (Buléon et al. 1984, Imberty et al. 1987). Montesanti et al. studied the influence of these parameters on the morphology of A-type single crystals prepared by precipitating narrow fractions of enzymatically-synthesized short-chain amylose by exposure to acetone vapors. Single crystals with well-defined facets were obtained by carefully selecting the fractions according to their average degree of polymerization (DP) and the width of the DP distribution (Montesanti et al. 2010).

Short-chain A-amylose single crystals are remarkable objects in many ways. First, to our knowledge, they have no equivalent in terms of size compared to those prepared from bio- or petrosourced polymers, as they can typically reach 10 μm in length and 200 nm in thickness (Montesanti et al. 2010). For this reason, their molecular structure was refined from high-resolution datasets collected from several single crystals probed with a synchrotron X-ray microbeam (Popov et al. 2009). While the broad structural features previously determined by Imberty et al. were confirmed (Imberty et al. 1987), it was shown that the number of water molecules accommodated in the crystal was twice that previously proposed, forming water-rich pockets between the slightly distorted amylose double helices.

Second, A-type amylose crystals grow axially. They are constituted of stacked lamellae in which all double helices are oriented along the growth direction (Imberty et al. 1987,

Montesanti et al. 2010). This feature is different from that of a majority of flexible polymers which form lamellar single crystals from dilute solutions, a few micrometer-wide but a few nanometer-thick, and involve chain-folding (Bassett et al. 1964, Keller 1968). In particular, when crystallized in the presence of a wide range of small hydrophobic molecules, long-chain amylose forms lamellar single helical inclusion complexes, referred to as V-type, in which guest molecules can be entrapped in the hydrophobic cavity of the amylose helices and between them (Brisson et al. 1991, Lourdin et al. 2015, Le et al. 2018, Nishiyama et al. 2010, Tan and Kong 2020, Le et al. 2021). In most cases, when crystallized *in vitro* from dilute solutions, short-chain polysaccharides, such as cellulose (Buléon et al. 1978, Buléon et al. 1980, Helbert et al. 1998), chitin (Helbert et al. 1998), or $\beta(1,4)$ -xylan (Chanzy et al. 1979), also form lamellar single crystals but the molecules are oriented perpendicularly to the lamella plane in which they adopt antiparallel arrangements (Chanzy and Vuong 1985). Depending on the crystallization conditions, low molecular weight $\beta(1,4)$ -mannan crystallizes into lamellae (Chanzy et al. 1984, Chanzy et al. 1987, Grimaud et al. 2019) or long rods (Chanzy et al. 1984) but in the latter case, it was shown that the molecules were oriented perpendicular to the growth axis (Bittiger and Husemann 1972, Heux et al. 2005).

Third, A-amylose single crystals are chemically polar objects. The double helices are constituted of parallel amylose chains with reducing and non-reducing ends, and the double helices are packed in a parallel fashion in the acicular crystals. By combining results from synchrotron X-ray and electron crystallography of single crystals, it was shown that the crystals grow in the direction of the reducing end of the amylose chains (Popov et al. 2009, Putaux et al. 2011). B-amylose has also been described by the packing of 6-fold parallel double helices in a hexagonal unit cell (Imberty et al. 1988, Takahashi et al. 2004). However, the formation of B-type amylose lamellar crystals was only reported once (Buléon et al. 1984) and, so far, it has not been possible to grow single crystals as large as those of A-amylose. Hexagonal lamellar crystals formed *in vitro* from enzymatically synthesized $\beta(1,3)$ -glucan might also exhibit chemically polar surfaces. However, whether triple helices are parallel or antiparallel in the unit cell is still a matter of debate (Deslandes et al. 1980, Ogawa et al. 2014, Pylkkänen et al. 2022). In addition, since the double helices are parallel in A-amylose and its monoclinic unit cell is noncentrosymmetric, A-type starches yield a strong signal in sum frequency generation spectra (Kong et al. 2014). Galvis et al. have studied the polarized Raman spectroscopy anisotropic response of short-chain A-type single crystals and have shown that the anisotropic response of the 865 cm^{-1} band of the glycosidic linkage was maximum when the polarization of the laser was oriented along the long axis of the crystals, i.e., parallel to the double helix axis. This

property was used to determine molecular orientation maps of ordered regions in native starch granules (Galvis et al. 2016).

In order to shed more light on the crystallization mechanisms of A-amylose, the present paper is a descriptive study of the impact of amylose concentration, crystallization temperature, and type of precipitant on the morphology of single crystals and their assemblies prepared from narrow fractions of short-chain amylose biosynthesized *in vitro*. The fractions were selected according to the previous results of Montesanti et al. (2010) in order to form faceted single crystals with a clearly recognizable habit.

Experimental section

Synthetic amylose fractions. Linear $\alpha(1,4)$ -D-glucan chains were synthesized *in vitro* from sucrose as glucosyl donor by the purified recombinant amylosucrase from *Neisseria polysaccharea*, under the conditions described in a previous article (Montesanti et al. 2010). The reaction products (fructose and maltooligosaccharides with a DP ranging from 2 to 36) were subsequently fractionated by preparative gel filtration. The DP distribution of each resulting fraction of short amylose chains was determined by high-performance anion-exchange chromatography with pulsed amperometric detection (HPAEC-PAD). In the following, these fractions are referred to as SAA (for "synthetic amylose amylosucrase"), associated with their minimum and maximum DP values, respectively. They are characterized by their number- and weight-average mean DPs (\overline{DP}_n and \overline{DP}_w , respectively) and polydispersity index $P = \overline{DP}_w / \overline{DP}_n$. In this study, two fractions have been considered. Fraction SAA14–21 ($\overline{DP}_n = 17.5$, $\overline{DP}_w = 17.6$, $P = 1.005$) has been used to study the effect of amylose concentration and crystallization temperature, while fraction SAA16–22 ($\overline{DP}_n = 19.1$, $\overline{DP}_w = 19.2$, $P = 1.004$) was crystallized in the presence of an inductive surface. Previous studies had shown that both fractions crystallized in the presence of acetone vapors would yield very similar crystals in terms of morphology and size.

Crystallization. Aqueous dispersions of amylose (0.05 to 5.0 % w/v) were crystallized according to a previously described protocol (Montesanti et al. 2010). The dispersions were heated in sealed vials at 150 °C for 15 min, cooled down to 80 °C and poured into a three-neck glass balloon pre-heated at 50–60 °C in an oil bath. Acetone (purchased from Sigma Aldrich, boiling temperature: 56 °C) was heated at 60 °C in a separate compartment connected to the balloon containing amylose by a heated glass tube, and the resulting vapor diffused into the amylose solution under gentle stirring. For experiments with acetone, the temperature of the

reactor was kept at 50, 55 or 58 °C to limit the evaporation of acetone from the medium. In order to reach a slightly higher crystallization temperature (60 °C), ethanol (purchased from Sigma Aldrich, boiling temperature: 78 °C) was used instead. The amylose solution was probed with a laser pointer and the onset of crystallization ($t = 0$) was defined as the time when the laser beam became visible, as turbidity developed in the suspension upon crystal formation. After 90 min, the mixtures were allowed to slowly cool down to room temperature, and the crystals were kept at 4 °C in their mother liquor.

To study the influence of an inductive substrate, a 2.6×7.6 cm glass slide was immersed in a 0.05% w/v SAA16–22 solution poured into the three-neck balloon and kept at 60 °C. An excess of preheated liquid acetone was added at once in the mixture that was kept at 50 °C for 90 min, then cooled down and kept at room temperature overnight. The glass slide was retrieved and allowed to air-dry before being sputter-coated with Au/Pd for scanning electron microscopy (SEM) observation.

Optical and scanning electron microscopy. Drops of crystal suspensions were deposited onto glass slides and observed between crossed polars at a magnification of 40× with a Zeiss Axiophot II microscope equipped with a retarding λ -waveplate to generate polarization colors. Images were recorded with an Olympus SC50 digital camera. For scanning electron microscopy (SEM), drops of the suspensions were allowed to air-dry on copper stubs or mica disks. The specimens were coated with Au/Pd and observed in secondary electron mode using a JEOL JSM-6100 microscope operating at an accelerating voltage of 8 kV or a Thermo Scientific FEI Quanta 250 microscope equipped with a field-emission gun (FEG) and operating at 2.5 kV.

Size and aspect ratio measurement. A particle size analysis was carried out from SEM images by measuring independently the length L and width w of populations of single crystals using the ImageJ software. The maximum width was considered for spindle-shaped crystals. Since the anisometric crystals were randomly oriented on the supporting stubs, it was easier to find crystals properly oriented to measure the length while it was more difficult to find crystals lying flat and allowing a reliable measurement of the width. The average length and width \bar{L} and \bar{w} were calculated from about 100 and 50 crystals, respectively. An average axial aspect ratio was defined as:

$$\bar{\rho}_1 = \frac{\bar{L}}{\bar{w}} \quad (1)$$

A second approach consisted in measuring (L_i, w_i) for each crystal and calculating an average axial aspect ratio $\overline{\rho_2}$ as:

$$\overline{\rho_2} = \frac{1}{N} \sum_i \frac{L_i}{w_i} \quad (2)$$

For each sample, 30-40 crystals were generally measured, as only crystals for which both length and width could be reliably measured were selected.

Results

In most of our crystallization experiments, A-amylose single crystals grew in the form of two main arrangements, namely, rosettes and fan-like assemblies (**Fig. 1a**). On the one hand, rosettes are quasi-spherical organizations of individual elongated platelets of identical size that grew radially from a common nucleus. In one rosette, the crystals do not seem to have a specific crystallographic orientation with respect to one another. Their apical end is flat and when the crystals are oriented parallel to the observation axis, their cross-section is a parallelogram with an obtuse angle of 118–123° that was assumed to be homothetic to the (a, b) plane of the monoclinic A-type unit cell (**Fig. 1d**) (Popov et al. 2009, Putaux et al. 2011). The orientation of this parallelogram with respect to the growth axis was the same for the crystals observed in all studied systems and independent of the crystallization conditions. On the other hand, fan-like assemblies can be described by a distribution of crystals that grew symmetrically with respect to the longest central crystal (**Fig. 1a**). The length of this central crystal can reach several tens of micrometers. The size of the crystals decreases from the central to the peripheral crystals of the assemblies, which suggests that they grew sequentially, likely formed by heterogeneous nucleation on the (010) face of a neighboring crystal (Putaux et al. 2011). However, they are not perfectly parallel to each other, which is probably due to the initial curvature at the tip of the crystal on top of which they nucleate, which promotes a steric divergence upon growing. There is also a rotation angle between the growth axes of the series of crystals in a fan. The origin of this rotation, which creates feather-like arrangements (**Fig. 1e**), is not known, as its angle can vary from one assembly to another. In some rare cases, symmetrical assemblies of two fan-like groups of crystals were observed that likely developed from a common twinned nucleus (**Fig. 1f**). Such symmetrical assemblies are probably frequent but easily disrupted by the manipulation of the specimen and/or by the capillary forces upon drying, which would explain why individual fans were mostly observed. The birefringence colors of rosettes and fans observed in polarized light micrographs are consistent. The projection of the radial organization of single crystals in rosettes results in four main quadrants,

while the color of the crystals in fans is unique, provided that the rotation angle between crystals is small (**Fig. 1b,c**). The crystals are blue when oriented at approximately $+45^\circ$ with respect to the polarizer and yellow-orange when oriented at -45° . This means that the birefringence axis of A-type crystals is oriented parallel to the growth axis, i.e. along the double-helical axis.

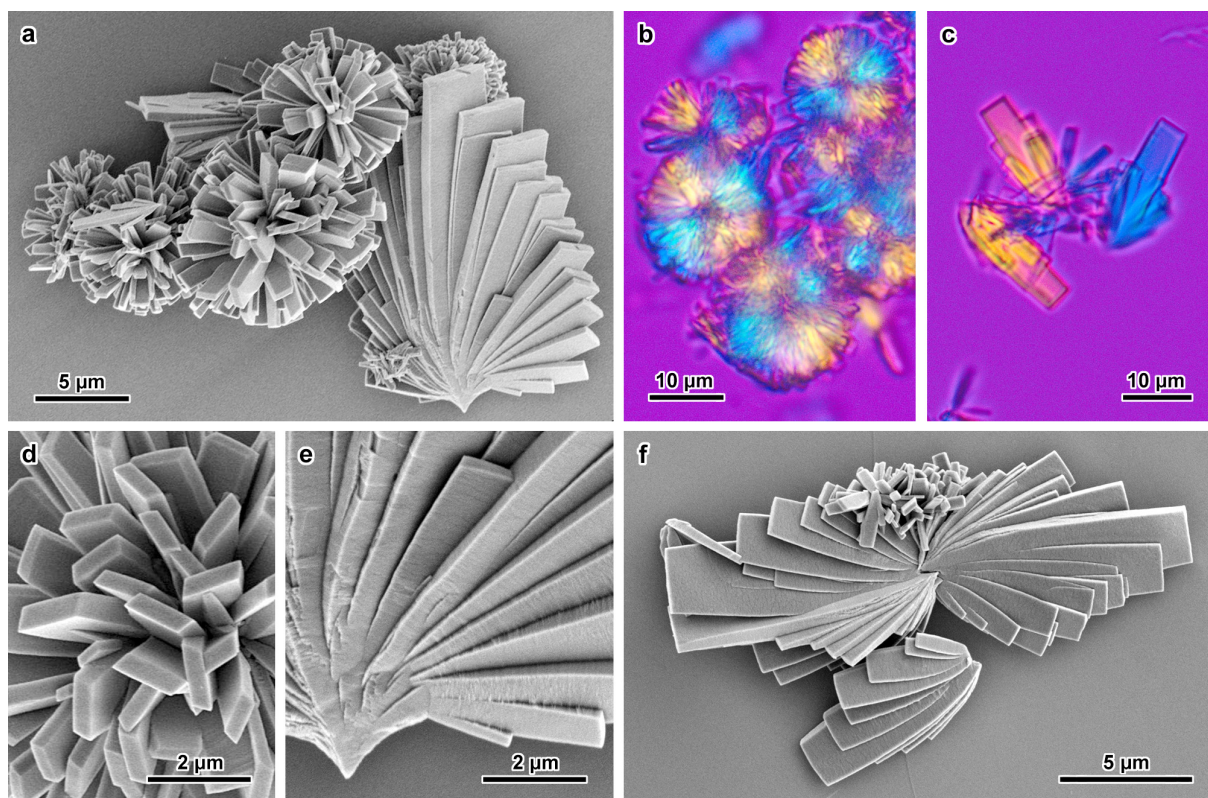


Figure 1. SEM images (a, d-f) and polarized light optical micrographs (b,c) of the rosettes and fan-shaped assemblies observed by crystallizing fraction SAA14–21 at 2% w/v by diffusion of acetone vapor at 55 °C: d) axial view of the single crystals in a rosette; e) detail of the nucleation region of the crystals in a fan-shaped assembly; f) symmetrical growth of twinned fan-shaped assemblies. The micrographs in (b) and (c) were recorded with a retarding λ -plate. The polarizer and analyzer are vertical and horizontal, respectively, with respect to the images.

Influence of the crystallization temperature

We have investigated the effect of the crystallization temperature on the morphology of crystals prepared from fraction SAA14–21 at a concentration of 0.05% w/v. Vapors of acetone were allowed to diffuse in amylose solutions kept at 50, 55 and 58 °C (**Fig. 2a-c**), while the solution was at 60 °C when in contact with ethanol (**Fig. 2d**). The SEM images show that the general morphological features of the crystals prepared in the four conditions are the same. The apical surface was flat and perpendicular to the growth direction ([Montesanti et al. 2010](#)). Additional SEM images and a polarized light optical micrograph of the crystals prepared with ethanol are shown in **Fig. S1**. In all cases, a large majority of more or less individual crystals that likely

resulted from the disruption of rosettes upon manipulation and drying forces was observed (**Fig. 2**). However, their dimensions, summarized in **Table 1**, are different. When \bar{L} and \bar{w} were determined independently, with acetone, the crystal average width remained stable (about 1.1 μm), while the length steadily increased with increasing crystallization temperature (from 5.6 to 9.7 μm at 50 and 58 $^{\circ}\text{C}$, respectively). With ethanol, the crystals were longer (10.1 μm) and thinner (0.7 μm), with a broader distribution. **Figure 3** shows plots of (L,w) dimensions simultaneously measured on selected crystals, for each crystallization temperature. The clouds were broadly ellipsoidal, which means that the length and width of the crystals were correlated. The slope of the linear regression was positive, i.e. the longer crystals were also wider. For the experiments performed with acetone, the clouds shifted to a higher length with increasing temperature while remaining within a similar range of width (**Fig. 3a-c**). For the crystals prepared with ethanol, the points were more scattered and the cloud was shifted to a lower and narrower width range (**Fig. 3d**). The average axial aspect ratios defined by **Eqs. 1** (ratio of the average length to the average width calculated independently) and **2** (average length-to-width ratio calculated for each crystal) were nearly identical (**Table 1**). The $\bar{\rho}_2$ average aspect ratio increased with increasing crystallization temperature (**Fig. 4b**). The higher value calculated for the sample crystallized with ethanol is consistent with the results obtained with acetone, in terms of influence of the incubation temperature on the aspect ratio of the crystals. However, since we did not conduct experiments with ethanol with the same amylose fraction at different temperatures, an effect of the nature of the solvent and its influence on the nucleation and growth of the crystals cannot be ruled out and deserves further investigation.

Table 1. Dimensions and aspect ratio of the A-type amylose crystals prepared from fraction SAA14–21 (0.05% w/v) at various temperatures and precipitant vapors, measured from SEM images. The standard deviation σ is given between brackets. \bar{L} and \bar{w} were determined independently. Aspect ratios $\bar{\rho}_1$ and $\bar{\rho}_2$ were defined by **Eqs. 1** and **2**.

Precipitant	T ($^{\circ}\text{C}$)	\bar{L} [σ] (μm)	\bar{w} [σ] (μm)	$\bar{\rho}_1$ [σ] (μm)	$\bar{\rho}_2$ [σ] (μm)
acetone	50	5.8 [1.6]	1.2 [0.3]	4.8 [2.5]	4.9 [0.8]
acetone	55	7.0 [1.4]	1.0 [0.2]	7.0 [2.8]	7.2 [0.8]
acetone	58	9.7 [1.0]	1.1 [0.2]	8.8 [2.5]	9.0 [1.1]
ethanol	60	10.1 [3.1]	0.7 [0.2]	14.4 [8.5]	14.4 [2.2]

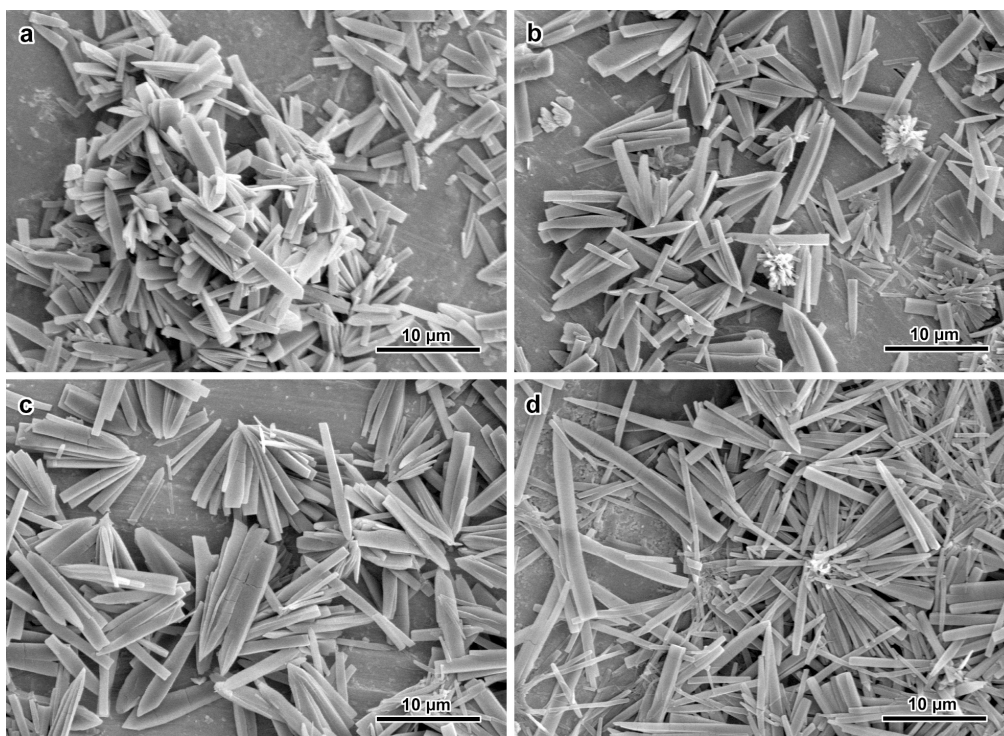


Figure 2. Influence of the crystallization temperature on the morphology of the A-type amylose single crystals prepared from fraction SAA14–21 (0.05% w/v) at 50 °C (a), 55 °C (b) and 58 °C (c) by diffusion of acetone vapors, and 60 °C (d) by diffusion of ethanol vapors (SEM images).

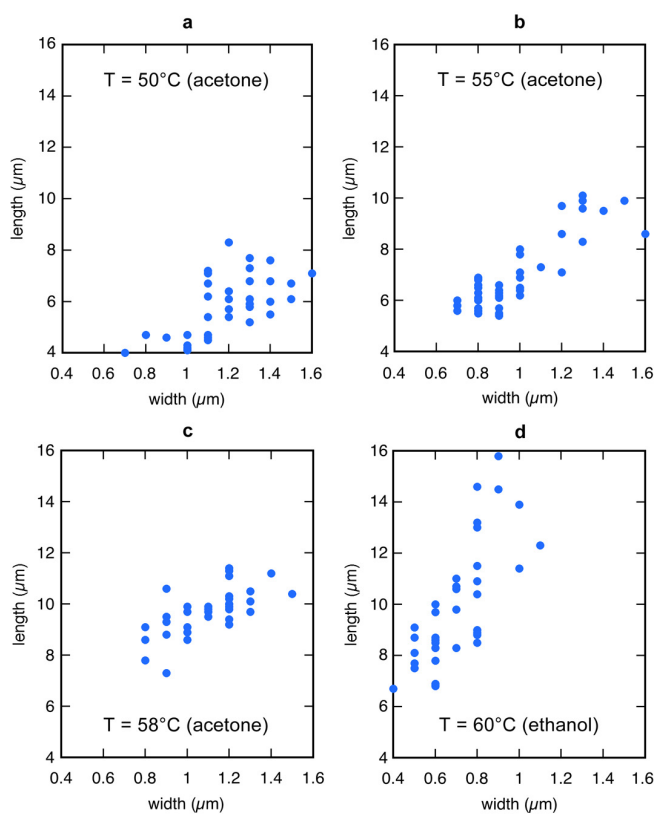


Figure 3. Length and width of a population of single crystals prepared from fraction SAA14–21 (0.05% w/v) at different temperatures by diffusion of acetone (a-c) or ethanol (d) vapors. The dimensions have been measured from SEM images.

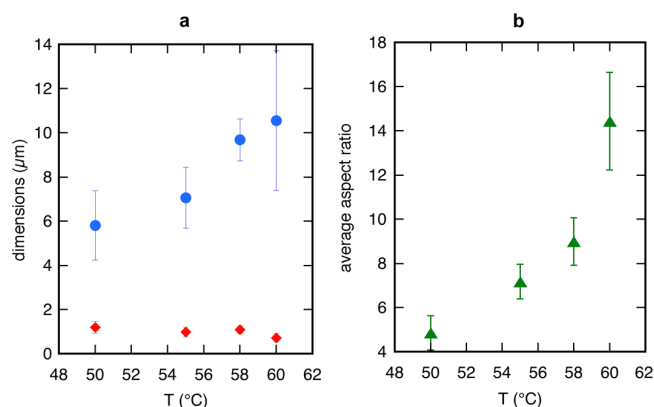


Figure 4. a) Average length (blue dots) and width (red lozenges) of crystals prepared from fraction SAA14–21 (0.05% w/v) as a function of crystallization temperature. The vertical bar corresponds to the standard deviation ($\pm \sigma$). b) Average axial aspect ratio $\overline{\rho_2}$ (see Eq. 2) of the crystals analyzed in Figure 3, as a function of crystallization temperature. Acetone vapors were used to crystallize amylose at 50, 55 and 58 °C, while ethanol vapors were used at 60 °C.

Influence of the amylose concentration

A series of samples from amylose solutions with increasing concentration was prepared (Table 1). Fraction SAA14–21 was crystallized at 0.05, 0.1, and 0.3 % w/v with acetone vapors and 5.0 % (w/v) with liquid acetone. As the amount of this fraction was limited and in order to complete the series of samples, we also crystallized fraction SAA16–22 at 1.0, 2.0 and 4.0% w/v. All experiments were performed at an incubation temperature of 55 °C. As seen in Figures 2b, 5a and S2a,b, at low amylose concentrations (0.05 and 0.3% w/v, respectively), the dominant crystal assemblies were rosettes, although a large number of them were disrupted by manipulation or drying, resulting in a majority of more or less individual crystals lying flat on the supporting stub. The relative number of fan-like assemblies significantly increased with increasing amylose concentration (Fig. 5b-d and S2c-d, 1.0-4.0% w/v, respectively).

When hot liquid acetone was added at once in a 5.0% w/v solution of SAA14-21, features of both rosettes and fans could be recognized in the resulting assemblies. The density of crystal packing significantly increased (Fig. 5e-h). The single crystals were organized into a quasi-spherical volume like in rosettes but, like in the fans previously described, groups of crystals defined separate "sectors" in which the crystals were more or less parallel to each other, likely due, to some extent, to an epitaxial nucleation on the large face of neighboring crystals.

The average length of the single crystals was calculated by measuring the diameter of the rosettes considered as spherical objects. For crystals prepared with acetone vapors, the average length and length distribution were rather independent of the concentration of amylose ($\bar{L} = 7.0 \pm 1.3 \mu\text{m}$, data not shown). The value significantly increased when liquid acetone was added to a 5.0% w/v amylose solution ($\bar{L} = 12.8 \pm 1.8 \mu\text{m}$).

To get a better impression of the three-dimensional organization of the crystals and their assemblies, several anaglyphs created from stereopairs of SEM images recorded with a tilt difference of 6° are proposed in **Figure S3**.

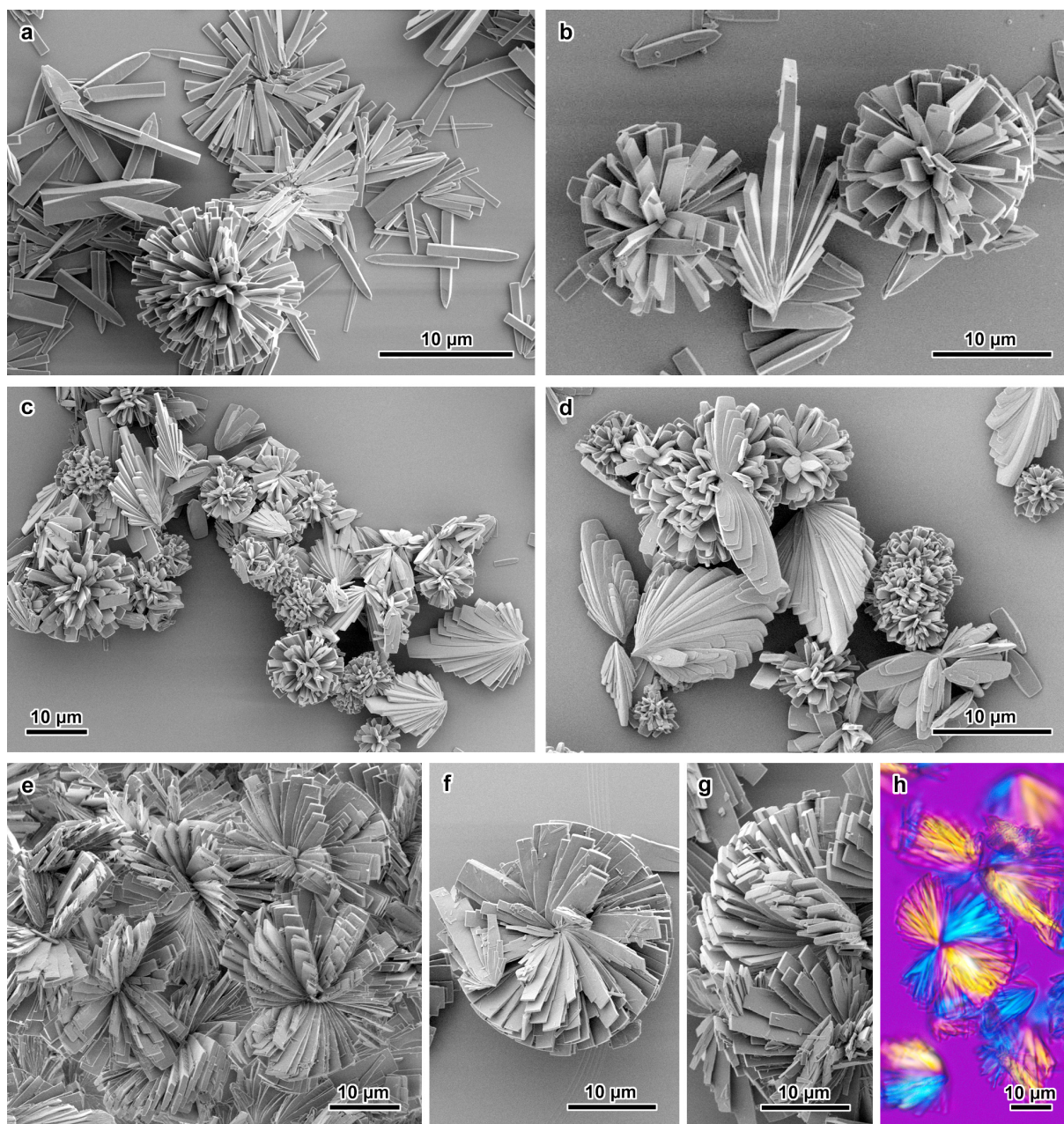


Figure 5. SEM images of the A-type amylose crystals prepared from fractions SAA14–21 at various concentrations at 0.3% w/v (a), 1.0% w/v (b), 2.0% w/v (c), 4.0% w/v (d), by diffusion of acetone vapor at 55 °C. e-h) Crystal assemblies formed by crystallizing fraction SAA14–21 at 5.0% w/v with liquid acetone at 55 °C. Image (h) is a polarized light optical micrograph recorded with a retarding λ -plate.

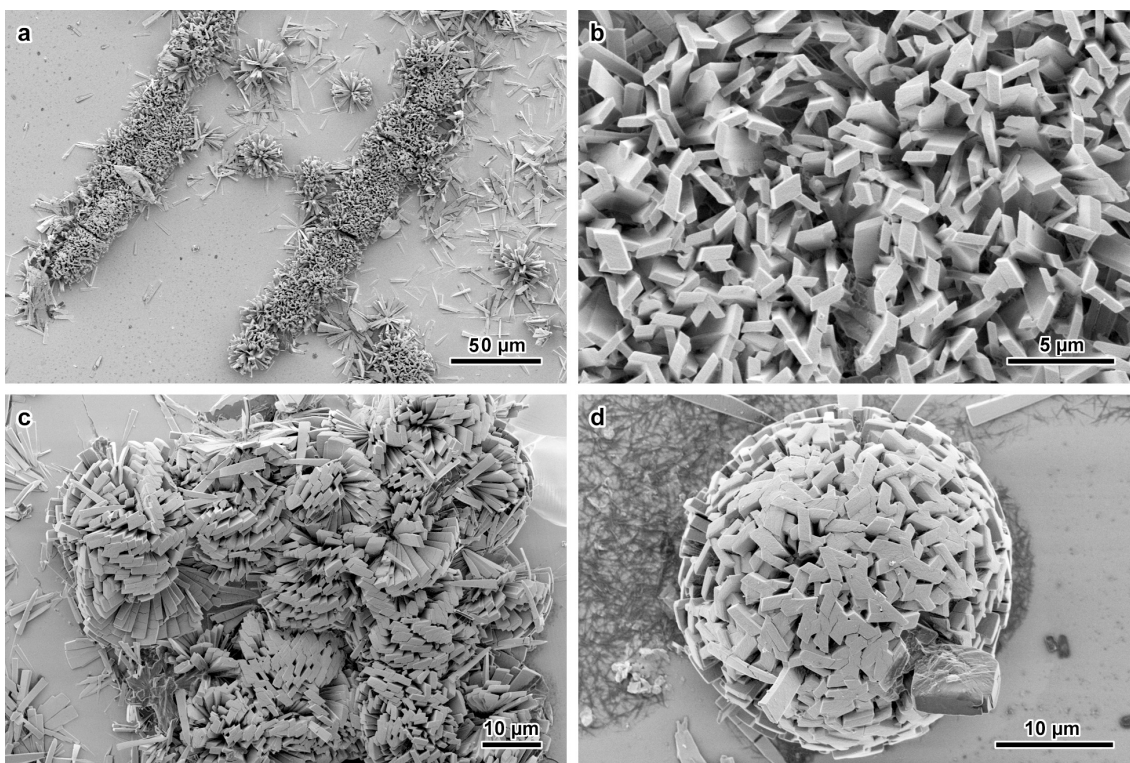


Figure 6. SEM images of A-type amylose assemblies observed by crystallizing fraction SAA16–22 at 0.05% w/v on a glass slide by addition of liquid acetone at 55 °C: a) low-magnification view of aligned assemblies of densely packed single crystals; b) enlargement of one region of image (a) showing single crystals that grew more or less perpendicularly to the glass slide surface; c) assembly of densely packed crystals; another region of the glass slide; d) spherical rosette containing densely packed crystals that grew radially from a common nucleus.

Influence of an inductive surface

In crystallization experiments from solutions, objects with specific shapes or surfaces can be used as "seeds" to favor heterogeneous nucleation and induce the formation of different crystal morphologies or orientations. A well-known example is the use of fibrils on which polymer lamellar crystals nucleate and grow perpendicularly to the fiber axis and form the so-called shish-kebab structure (Helbert and Chanzy 1994). In the present study, the induction effect of the surface of a glass slide was studied by crystallizing fraction SAA16-22 at 0.05% w/v by the addition of liquid acetone at 55 °C. The SEM image in **Figure 6a** shows that high concentrations of crystals formed along lines that likely correspond to defects on the glass slide surface. The higher magnification micrographs in **Figure 6b** show that these regions are dense arrays of crystals that grew more or less perpendicular to the glass slide surface. A large number of these crystals are seen in near axial view and seem to be randomly oriented around their growth axis with respect to one another. In other regions of the slide, the density of crystals is even higher (**Fig. 6c**). The crystals appear to have grown like in the rosette assemblies observed

by crystallizing amylose at 5.0% w/v with liquid acetone (**Fig. 5e-g**), although the concentration of the solution was significantly lower (0.05% w/v). The crystals are often in close contact, more or less parallel to each other or sometimes even interpenetrated (**Figs. 6c** and **S4a**). Densely packed crystals were also observed in spherical rosettes such as those shown in **Figures 6d** and **S4b**. The respective orientation of the crystals around their growth axis with respect to their close neighbors seems to be random, although some crystals partially merged.

Discussion

The diffusion of acetone vapors into the aqueous solution of short-chain amylose increased supersaturation and promoted the formation of nuclei ([Boistelle and Astier 1988](#)). Considering the two main forms of A-type crystal assemblies that were observed, different types of nuclei corresponding to clusters of amylose double helices may have spontaneously formed, one assembly or the other being favored by the crystallization conditions. Their geometry and chain organization are not known with precision although these early clusters likely contained several domains allowing to initiate the growth of crystals in various directions. Primary nucleation can be homogeneous in the amylose solution but heterogeneous nucleation on the walls of the glass balloon cannot be ruled out. At low amylose concentration, rosettes are the favored form of crystal assembly and likely result from homogeneous nucleation events. All crystals in one rosette have the same length and, therefore, they must have grown simultaneously and independently in various directions from a common nucleus. However, even when the rosettes were damaged by the manipulation and/or drying forces, like in **Figs. 5a** and **S1b**, resulting in a radial spread of the constituting single crystals, the shape of the nuclei could not be unambiguously identified.

As the initial concentration of amylose increases, secondary nucleation also occurs and results in the development of fan-like assemblies by successive nucleation events on both large faces of single crystals. The fact that the crystals in one fan do not randomly nucleate on these surfaces but rather at the base of the neighboring crystal suggests that the nucleation events occur in sequence and over a short timescale.

In our previous article, we proposed hypotheses based on classical polymer growth mechanisms to explain why axial growth was favored over lateral growth to form A-type acicular single crystals ([Putaux et al. 2011](#)). Two possible mechanisms can describe the formation of layers of amylose double helices in the (001) planes perpendicular to the growth axis ([Burton and Cabrera 1951](#), [Boistelle and Astier 1988](#)). On the one hand, according to the so-called "birth and spread" model, independent steps would nucleate, develop laterally and

merge on the (001) surface by addition of double helices. On the other hand, the layers would develop by a spiral propagation of steps around screw dislocations whose axis would be parallel to the growth axis. The resolution of the SEM images of the (001) surface was not high enough to detect such defects and favor one mechanism over the other although growth spirals were frequently observed in polymer lamellar crystals (Keller 1968, Le et al. 2021). In rosettes and fan-like assemblies, the crystals start growing with a triangular shape but rapidly adopt the parallelipetal shape of an elongated and thick platelet with a rather stable width and thickness. The (001) face thus appears to be less stable than the (010) and (100) faces parallel to the growth direction.

To our knowledge, the formation of similar rosettes and fan-like assemblies has not been reported for other polysaccharides crystallized *in vitro*, although spiky spherocrystals of enzymatically-synthesized short-chain cellulose have been described (Kobayashi et al. 2000). However, in this case, the cellulose chains were perpendicular to the growth axis of lamellar single crystals. Flower-like assemblies of radially grown rod-like crystals were more often observed with inorganic compounds, such as stibnite (Sb_2S_3) (An et al. 2003) or aragonite (CaCO_3) crystallized in the presence of urea and poly(N-vinyl pyrrolidone) (Hongxia et al. 2011). Dense spherulites can be formed by crystallizing long-chain (Ziegler et al. 2020) or short-chain (Ring et al. 1987, Cai et al. 2013) amylose from concentrated solutions. In particular, Helbert et al. prepared A-type spherocrystals by mixing 10 % w/v aqueous solutions of DP 15 amylose with ethanol at 78 °C followed by slow cooling (Helbert et al. 1993). Transmission electron microscopy images of ultrathin sections of resin-embedded particles showed that the spherocrystals were constituted of contiguous elongated crystalline domains radiating from the center. In addition, selected area electron diffraction patterns confirmed the radial orientation of the amylose double helices, in line with the positive optical birefringence of the spherocrystals.

Even at an amylose concentration of 5.0 % w/v and with the direct addition of liquid acetone, we did not observe solid spherocrystals. Individual platelet acicular single crystals could still be recognized even though they seemed to be distributed within a virtual spherical volume (Fig. 5e-g). The incorporation of an inductive surface in the crystallization medium promoted the formation of denser assemblies, even at significantly lower amylose concentration, but without reaching a full compacity (Figs. 6c,d and S4). The fact that rosettes are composed of a very large number of platelet single crystals clearly imposes a topological constraint: how can flat parallelipetal (i.e. not conical) units growing from a common nucleus fill a spherical volume?

On the one hand, a twist component around the growth axis might help the crystals to form more or less helical arrangements but they cannot ultimately form a sphere if all crystals have similar shape and size. Partially helical crystal distributions can be observed in fan-like assemblies (**Figs. 1a** and **5d**) as well as in dense rosettes formed at high amylose concentration (**Figs. 5e,f** and **S3c,d**). These assemblies can be all described as portions of left-handed spirals whose director points towards the viewer (**Fig. 7**). That the chirality of the assemblies is an expression at a higher lengthscale of the chirality of the nucleus and/or the monoclinic unit cell and constituting parallel left-handed double-helices remains an open question that deserves further investigation. Twisting was indeed observed in native cellulose I nanofibrils described as axial associations of parallel chains of $\beta(1,4)$ -linked glucosyl units (Ogawa 2019).

On the other hand, the nucleation and growth of successive generations of smaller crystals would gradually fill the cavities. However, that was only partially observed in our system, as the crystals tended to nucleate close to the center of the assemblies and diverge upon growing (**Figs. 5e-g** and **S3c,d**). Stacks of confined plates were favored and the rosettes thus appeared to be organized in "sectors" in which the crystals kept some orientation with respect to one another other due to the combined effects of early steric hindrance and growth with a rather constant thickness.

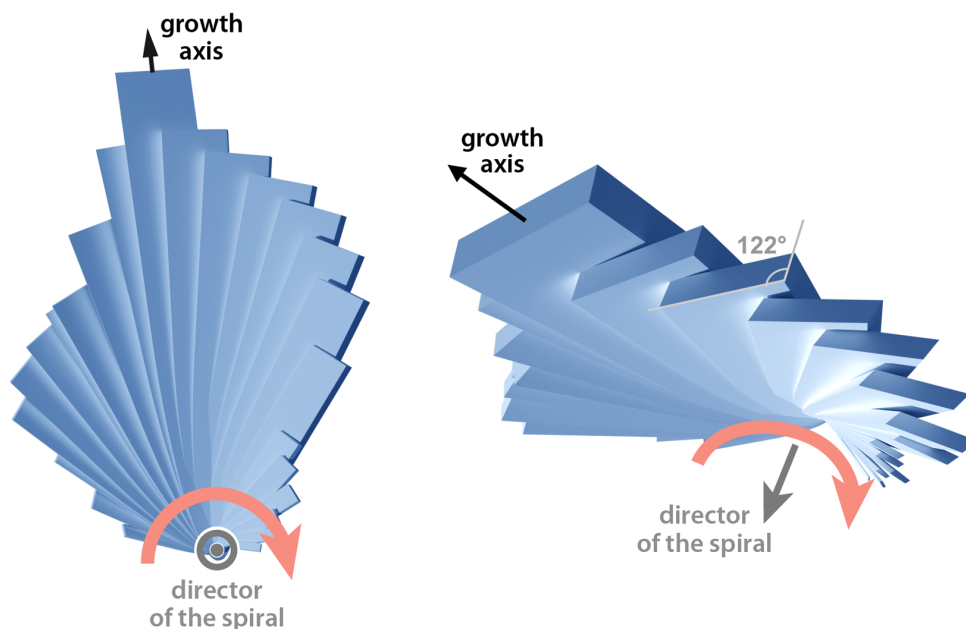


Figure 7. Artist views showing the left-handed spiral organization of A-amylose single crystals in a fan-like assembly.

Conclusion

Montesanti et al. (2010) showed that the morphology of A-type single crystals and their assemblies strongly depend on parameters such as average DP and length distribution of the amylose fraction. In the present study, we have selected two narrow fractions of enzymatically-synthesized linear amylose according to their ability to form single crystals with a well-defined faceted morphology that could be related to the unit cell of the constituting allomorph. Different short-chain amylose fractions would likely induce different nucleation and growth mechanisms although, so far, only acicular single crystals have been reported for allomorph A (Buléon et al. 1984, Imberty et al. 1988, Montesanti et al. 2010). We have assessed the impact of amylose concentration, method of addition of the precipitant (vapors or liquid) and crystallization temperature on the morphology of the crystal assemblies. A higher crystallization temperature promotes the axial growth of the crystals, resulting in a higher aspect ratio. For a given set of crystallization conditions, the width and length of the individual crystals are correlated, although we did not consider the thickness of the single crystals for practical reasons explained in the experimental section. The relative fraction of rosettes with respect to fan-like assemblies increases with increasing initial amylose concentration, suggesting that the nucleation and development of new rosettes is favored over the growth of existing crystals. Within the range of concentration explored in this work, no solid spherulites were observed. Concentrations higher than 5.0 % w/v should thus be tested to see if such particles can indeed be formed from narrow fractions of short-chain amylose.

Preliminary results on the use of an inductive surface to promote heterogeneous nucleation showed that extremely dense crystal organizations could be achieved, even at low amylose concentration. One remarkable peculiarity of such organizations is that, considering the molecular polarity of the single crystals resulting from the parallel packing of amylose double helices, relatively large surfaces exposing a high density of reducing chain ends are accessible to specific chemical labeling or grafting. Using inductive surfaces with a different chemical composition or rugosity, and native or patterned surface defects, may allow for controlling the orientation and distribution of single crystals. Other nucleating agents like nanoparticles (e.g. starch nanoparticles from acid-hydrolyzed native granules) and nanofibrils (e.g. cellulose, chitin or carbon nanotubes, to form so-called shish-kebab organizations) can be tested as well.

As previously mentioned, A-type amylose single crystals have rather unique features in terms of morphology and size in the field of polymer crystallization. Further studies should be conducted in order to understand if and how the morphogenesis of these crystals is specific to

amylose and whether this knowledge can be transposed to grow large polysaccharide single crystals suitable for X-ray microcrystallography.

Acknowledgments

The Marie Curie Early Stage Research Training Fellowship of the European Community's 6th Framework Programme (grant agreement #MEST-CT-2004-503322) is acknowledged for the partial financial support of N.M.'s PhD. We thank Pierre-Claude Escalier (TBI) for his help in preparing the fractions of short-chain amylose, Pierre Sailer (CERMAV) for the 3D models of crystal assemblies, Danièle Dupeyre (CERMAV) for assistance with SEM imaging, and the NanoBio-ICMG platform (UAR 2607, Grenoble) for granting access to the Electron Microscopy facility. CERMAV is part of Institut Carnot PolyNat (grant agreement #ANR-11-CARN-030-01) and the Glyco@Alps programme (grant agreement #ANR-15-IDEX-02).

References

- An C, Tang K, Yang Q, Qian Y (2003) Formation of crystalline stibnite bundles of rods by thermolysis of an antimony(III) diethyldithiocarbamate complex in ethylene glycol. *Inorg Chem* 42:8081–8086. <https://doi.org/10.1021/ic034534n>
- Bassett DC, Dammont FR, Salovey R (1964) On the morphology of polymer crystals. *Polymer* 5:579–588. [https://doi.org/10.1016/0032-3861\(64\)90208-3](https://doi.org/10.1016/0032-3861(64)90208-3)
- Boistelle R, Astier J-P (1988) Crystallization mechanisms in solution. *J Cryst Growth* 90:14–30. [https://doi.org/10.1016/0022-0248\(88\)90294-1](https://doi.org/10.1016/0022-0248(88)90294-1)
- Bittiger H, Husemann E (1972) Crystal morphology of precipitated mannan. *Polym Lett* 10:367–371. <https://doi.org/10.1002/pol.1972.110100507>
- Brisson J, Chanzy H, Winter WT (1991) The crystal and molecular structure of V_H amylose by electron diffraction analysis. *Int J Biol Macromol* 13:31–39. [https://doi.org/10.1016/0141-8130\(91\)90007-H](https://doi.org/10.1016/0141-8130(91)90007-H)
- Buléon A, Chanzy H (1978) Single crystals of cellulose II. *J Polym Sci Part B Polym Phys* 16:833–839. <https://doi.org/10.1002/pol.1978.180160508>
- Buléon A, Chanzy H (1980) Single crystals of cellulose IV_{II}: Preparation and properties. *J Polym Sci* 18:1209–1217. <https://doi.org/10.1002/pol.1980.180180604>
- Buléon A, Duprat F, Booy FP, Chanzy H (1984) Single crystal of amylose with a low degree of polymerization. *Carbohydr Polym* 4:161–173. [https://doi.org/10.1016/0144-8617\(84\)90009-2](https://doi.org/10.1016/0144-8617(84)90009-2)
- Buléon A, Potocki-Véronèse G, Putaux J-L (2007) Self-association and crystallization of amylose. *Aust J Chem* 60:706–718. <https://doi.org/10.1071/CH07168>
- Burton WK, Cabrera N, Frank CF (1951) The growth of crystals and the equilibrium structure of their surfaces. *Phil Trans Roy Soc Lond A, Math Phys Sci* 243:299–358. <https://doi.org/10.1098/rsta.1951.0006>
- Cai L, Shi Y-C (2013) Self-assembly of short linear chains to A- and B-type starch spherulites and their enzymatic digestibility. *J Agric Food Chem* 61:10787–10797. <https://dx.doi.org/10.1021/jf402570e>

- Chanzy H, Dubé M, Marchessault RH (1979) Structural polymorphism of (1→4)-β-D-xylan. *Polymer* 20:1037–1039. [https://doi.org/10.1016/0032-3861\(79\)90205-2](https://doi.org/10.1016/0032-3861(79)90205-2)
- Chanzy HD, Grosrenaud A, Vuong R, Mackie W (1984) The crystalline polymorphism of mannan in plant cell walls and after recrystallisation. *Planta* 161:320–329. <https://doi.org/10.1007/BF00398722>
- Chanzy H, Perez S, Miller DP, Paradossi G, Winter WT (1987) An electron diffraction study of the mannan I crystal and molecular structure. *Macromolecules* 20:2407–2413. <https://doi.org/10.1021/ma00176a014>
- Chanzy H, Vuong R (1985) Ultrastructure and morphology of crystalline polysaccharides, in "Polysaccharides: Topics in Structure and Morphology", Atkins EDT ed, Macmillan Press Ltd, London, pp 41–71.
- Deslandes Y, Marchessault RH, Sarko A (1980) Triple-helical structure of (1→3)-β-D-glucan. *Macromolecules* 13:1466–1471. <https://doi.org/10.1021/ma60078a020>
- Galvis L, Bertinetto C, Putaux J-L, Montesanti N, Vuorinen, T (2016) Orientation mapping of crystallites in starch granules performed by polarized Raman spectroscopy (PRS). *Carbohydr Polym* 154:70–76. <https://doi.org/10.1016/j.carbpol.2016.08.032>
- Gidley MJ (1987) Factors affecting the crystalline type (A-C) of native starches and model compounds: a rationalization of observed effects in terms of polymorphic structures. *Carbohydr Res* 161:301–304. [https://doi.org/10.1016/S0008-6215\(00\)90087-9](https://doi.org/10.1016/S0008-6215(00)90087-9)
- Grimaud F, Pizzut-Serin S, Tarquis L, Ladevèze S, Morel S, Putaux J-L, Potocki-Veronese G (2019) In vitro synthesis and crystallization of β-1,4-mannan. *Biomacromolecules* 20:846–853. <https://doi.org/10.1021/acs.biomac.8b01457>
- Helbert W, Chanzy H (1994) Oriented growth of V amylose n-butanol crystals on cellulose. *Carbohydr Polym* 24:119–122. [https://doi.org/10.1016/0144-8617\(94\)90021-3](https://doi.org/10.1016/0144-8617(94)90021-3)
- Helbert W, Chanzy H, Planchot V, Buléon A, Colonna P (1993) Morphological and structural features of amylose spherocrystals of A-type. *Int J Biol Macromol* 15:183–187. [https://doi.org/10.1016/0141-8130\(93\)90021-d](https://doi.org/10.1016/0141-8130(93)90021-d)
- Helbert W, Sugiyama J (1998) High-resolution electron microscopy on cellulose II and α-chitin single crystals. *Cellulose* 5:113–122. <https://doi.org/10.1023/A:1009272814665>
- Heux L, Hägglund P, Putaux J-L, Chanzy H (2005) Structural aspects in semicrystalline samples of the mannan II family. *Biomacromolecules* 6:324–332. <https://doi.org/10.1021/bm0495349>
- Hongxia G, Zhenping Q, Peng Q, Peng Y, Suping C, Wei W (2011) Crystallization of aragonite CaCO₃ with complex structures. *Adv Powder Technol* 22:777–783. <https://doi.org/10.1016/j.appt.2010.11.004>
- Imberty A, Chanzy H, Pérez S, Buléon A, Tran V (1987) New three-dimensional structure for A-starch. *Macromolecules* 20:2634–2636. <https://doi.org/10.1021/ma00176a054>
- Imberty A, Chanzy H, Pérez S, Buléon A, Tran V (1988) The double-helical nature of the crystalline part of A-starch. *J Mol Biol* 201:365–384. [https://doi.org/10.1016/0022-2836\(88\)90144-1](https://doi.org/10.1016/0022-2836(88)90144-1)
- Keller A (1968) Polymer crystals. *Rep Prog Phys* 31:623–704. <https://doi.org/10.1088/0034-4885/31/2/304>
- Kobayashi S, Hobson LJ, Sakamoto J, Kimura S, Sugiyama J, Imai T, Itoh T (2000) Formation and structure of artificial cellulose spherulites via enzymatic polymerization. *Biomacromolecules* 1:168–173. <https://doi.org/10.1021/bm990010w>

- Kong L, Lee C, Kim SH, Ziegler GR (2014) Characterization of starch polymorphic structures using vibrational sum frequency generation spectroscopy. *J Phys Chem B* 118:1775–1783. <https://doi.org/10.1021/jp411130n>
- Le CAK, Choisnard L, Wouessidjewe D, Putaux J-L (2018) Polymorphism of crystalline complexes of amylose with fatty acids. *Int J Biol Macromol* 119:555–564. <https://doi.org/10.1016/j.ijbiomac.2018.07.163>
- Le CAK, Choisnard L, Wouessidjewe D, Putaux J-L (2021) Polymorphism of V-amylose cocrystallized with aliphatic diols. *Polymer* 213:123302. <https://doi.org/10.1016/j.polymer.2020.123302>
- Lourdin D, Putaux J-L, Potocki-Veronese G, Chevigny C, Roland-Sabaté A, Buléon A (2015) Crystalline structure in starch. In "Starch - Metabolism and Structure", Nakamura Y ed., Springer Japan, pp 61–90 –https://doi.org/10.1007/978-4-431-55495-0_3
- Montesanti N, Véronèse G, Buléon A, Escalier P-C, Kitamura S, Putaux J-L (2010) A-type crystals from dilute solutions of short amylose chains. *Biomacromolecules* 11:3049–3058. <https://doi.org/10.1021/bm1008712>
- Nishiyama Y, Mazeau K, Morin M, Cardoso MB, Chanzy H, Putaux J-L (2010) Molecular and crystal structure of 7-fold V-amylose complexed with 2-propanol. *Macromolecules* 43:8628–8636. <https://doi.org/10.1021/ma101794w>
- Ogawa Y (2019). Electron microdiffraction reveals the nanoscale twist geometry of cellulose nanocrystals. *Nanoscale* 11:21767–21774. <https://doi.org/10.1039/c9nr06044h>
- Ogawa Y, Noda K, Kimura S, Kitaoka M, Wada M (2014) Facile preparation of highly crystalline lamellae of (1→3)- β -D-glucan using an extract of *Euglena gracilis*. *Int J Biol Macromol* 64:415–419. <https://doi.org/10.1016/j.ijbiomac.2013.12.027>
- Ohdan K, Fujii K, Yanase M, Takaha T, Kuriki T (2006) Enzymatic synthesis of amylose. *Biocatal Biotransform* 24:77–81. <https://doi.org/10.1080/10242420600598152>
- Pérez S, Bertoft E (2010) The molecular structures of starch components and their contribution to the architecture of starch granules: A comprehensive review. *Starch/Stärke* 62:389–420. <https://doi.org/10.1002/star.201000013>
- Popov D, Buléon A, Burghammer M, Chanzy H, Montesanti N, Putaux J-L, Potocki-Véronèse G, Riekkel C (2009) Crystal structure of A-amylose: a revisit from synchrotron microdiffraction analysis of single crystals. *Macromolecules* 42:1167–1174. <https://doi.org/10.1021/ma801789j>
- Potocki de Montalk G, Remaud-Simeon M, Willemot R-M, Sarçabal P, Planchot V, Monsan P (2000) Amylosucrase from *Neisseria polysaccharea*: novel catalytic properties. *FEBS Lett* 471:219–223. [https://doi.org/10.1016/S0014-5793\(00\)01406-X](https://doi.org/10.1016/S0014-5793(00)01406-X)
- Putaux J-L, Montesanti N, Veronese G, Buléon A (2011) Morphology and structure of A-amylose single crystals. *Polymer* 52:2198–2205. <https://doi.org/10.1016/j.polymer.2011.03.014>
- Pylkkänen R, Mohammadi P, Liljeström V, Płaziński W, Beaune G, Timonen JVI, Penttilä M (2022) β -1,3-Glucan synthesis, novel supramolecular self-assembly, characterization and application. *Nanoscale* 14:15533–15541. <https://doi.org/10.1039/D2NR02731C>
- Ring SA, Miles MJ, Morris VJ, Turner R, Colonna P (1987) Spherulitic crystallization of short chain amylose. *Int J Biol Macromol* 9:158–160. [https://doi.org/10.1016/0141-8130\(87\)90044-4](https://doi.org/10.1016/0141-8130(87)90044-4)
- Takahashi Y, Kumano T, Nishikawa S (2004) Crystal Structure of B-Amylose. *Macromolecules* 37:6827–6832. <https://doi.org/10.1021/ma0490956>

- Tan L, Kong L (2020) Starch-guest inclusion complexes: Formation, structure, and enzymatic digestion. *Crit Rev Food Sci Nutr* 60:780–790.
<https://doi.org/10.1080/10408398.2018.1550739>
- Whittam MA, Noel TR, Ring SG (1990) Melting behaviour of A- and B-type crystalline starch. *Int J Biol Macromol* 12:359–362. [https://doi.org/10.1016/0141-8130\(90\)90043-A](https://doi.org/10.1016/0141-8130(90)90043-A)
- Ziegler GR (2020) Enzyme-resistant starch spherulites. *Starch* 72:1900217.
<https://doi.org/10.1002/star.201900217>

Supporting information

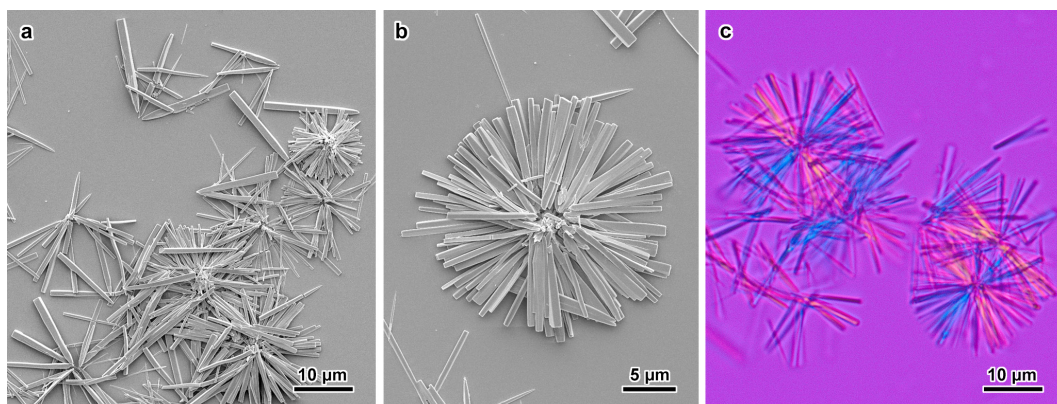


Figure S1. SEM images (a,b) and polarized light optical micrograph (c) of the single crystal assemblies observed by crystallizing fraction SAA14–21 at 0.05% w/v by diffusion of ethanol vapors at 60 °C. The image in (c) was recorded with a retarding λ -plate.

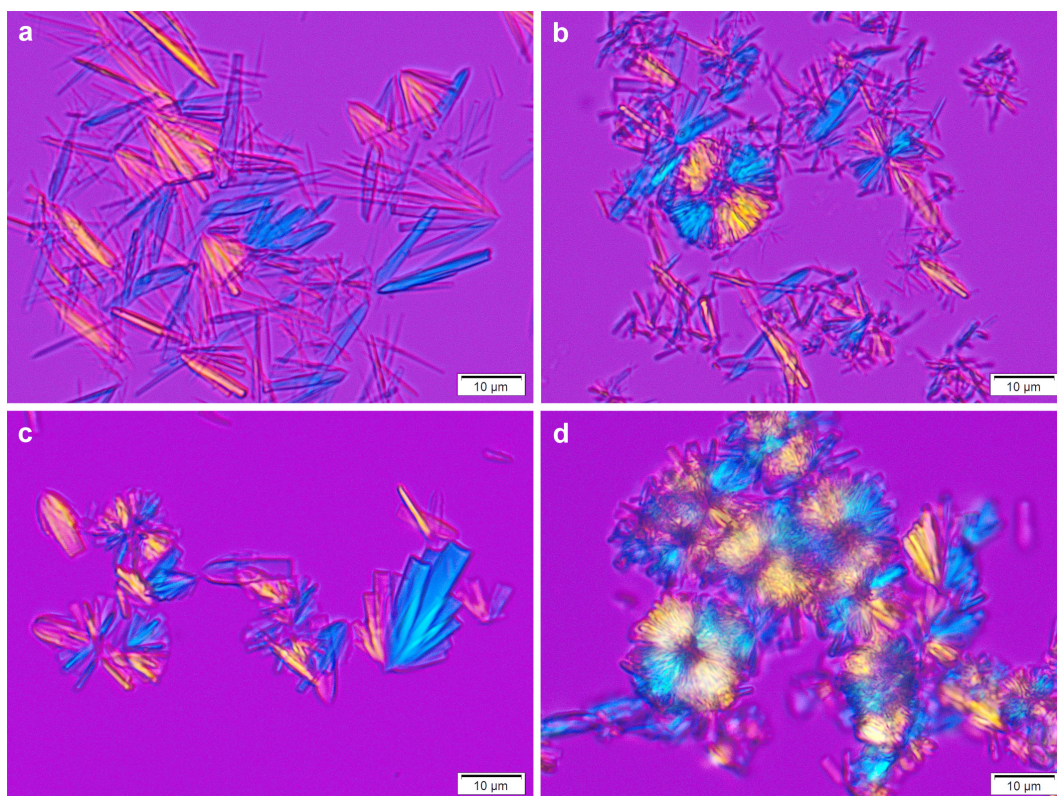
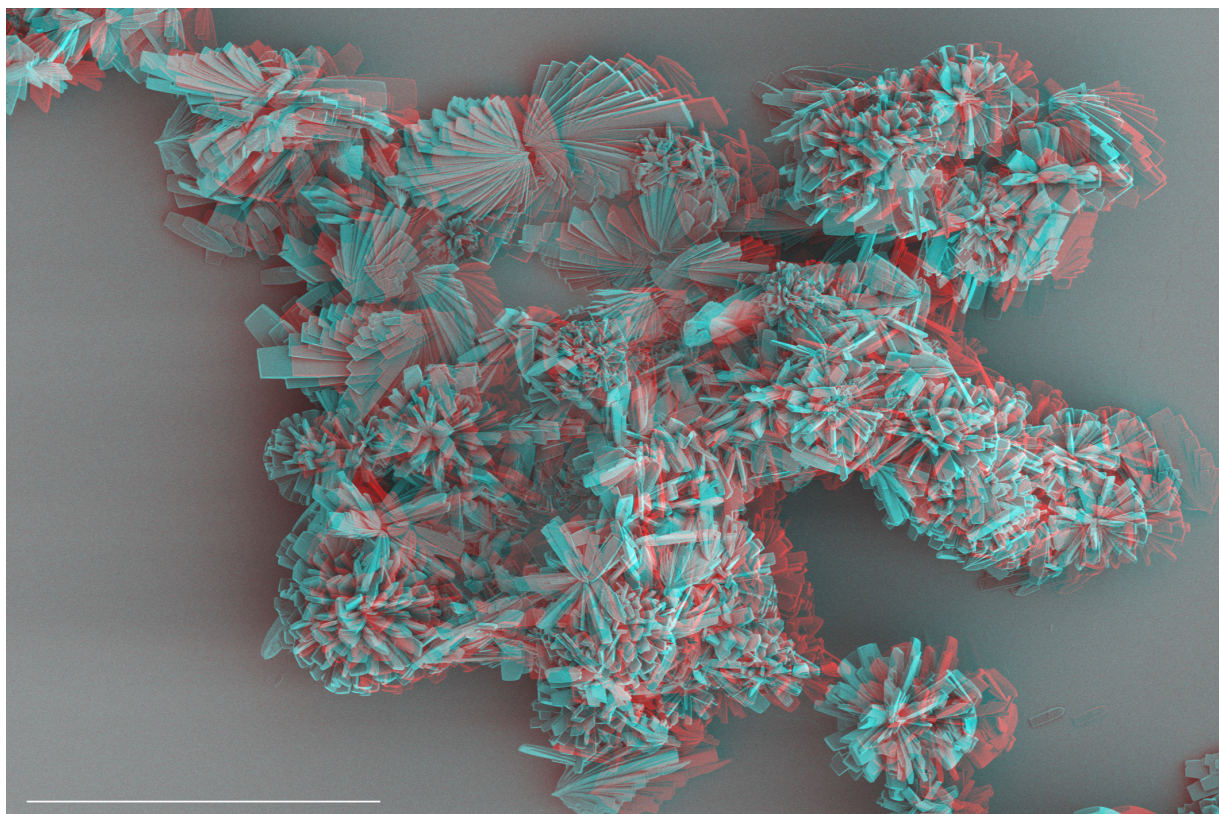
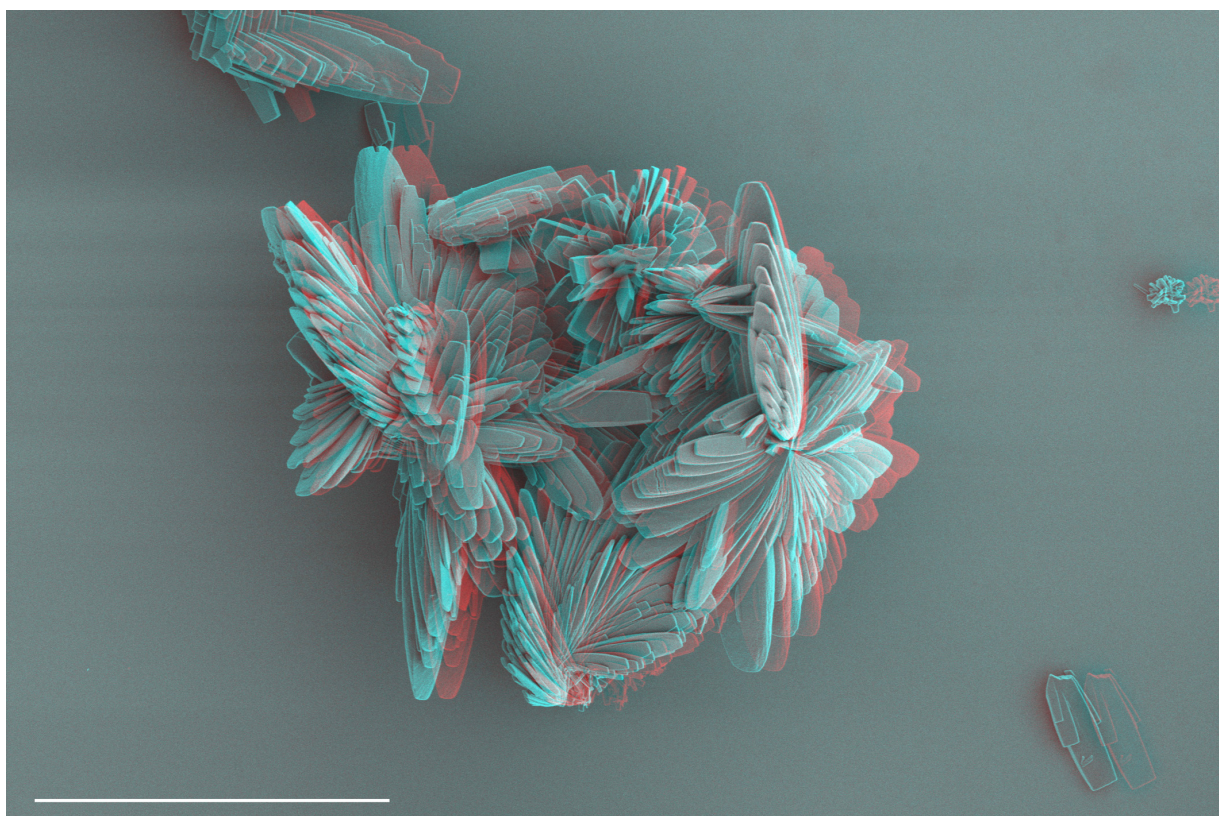


Figure S2. Influence of the initial concentration of SAA14–21 amylose fraction on the morphology of A-type crystals prepared by diffusion of acetone vapors at 55 °C: a) 0.05% w/v; b) 0.3% w/v; c) 1.0% w/v; d) 2.0% w/v. The polarized light optical micrographs were recorded with a retarding λ -plate.

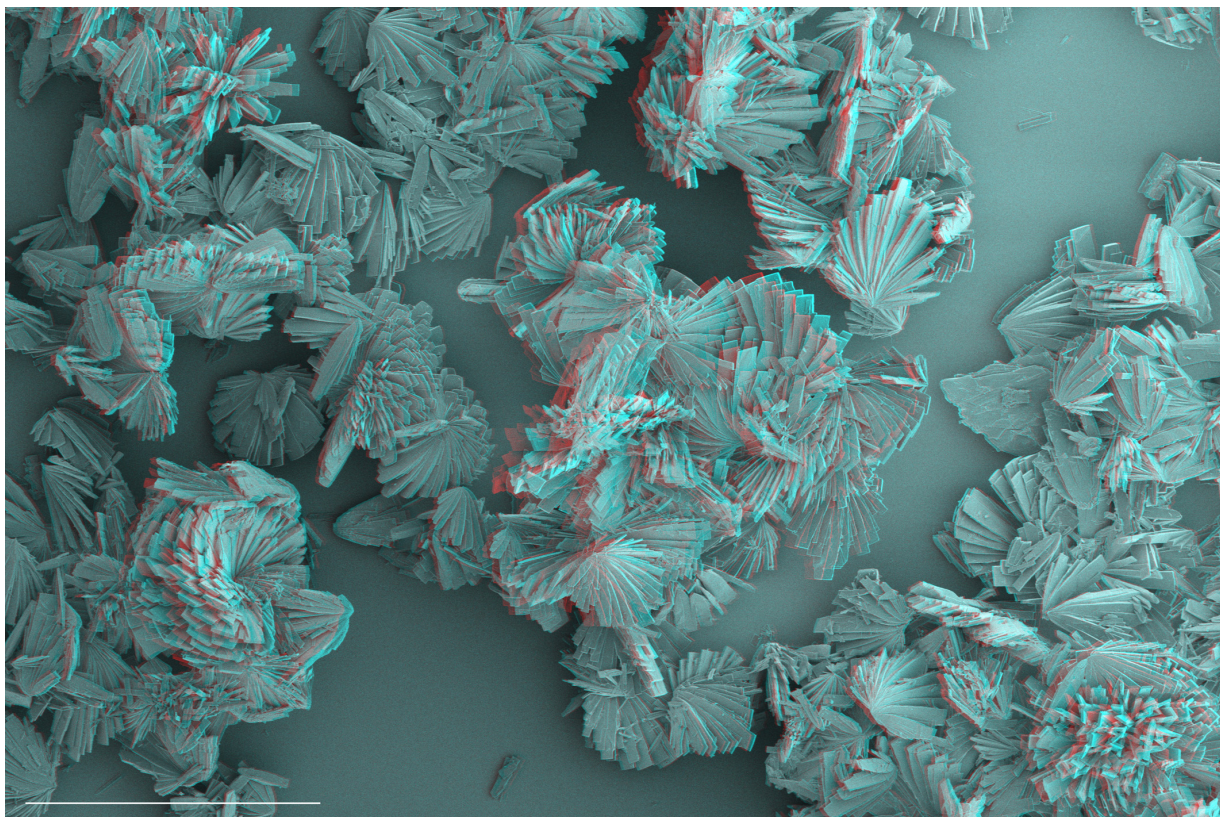
Figure S3. Anaglyphs created with the Thermo Scientific "xT microscope" software operating the Quanta 250 SEM (6° tilt angle between images). Color glasses setup: cyan on the left eye and red on the right eye.



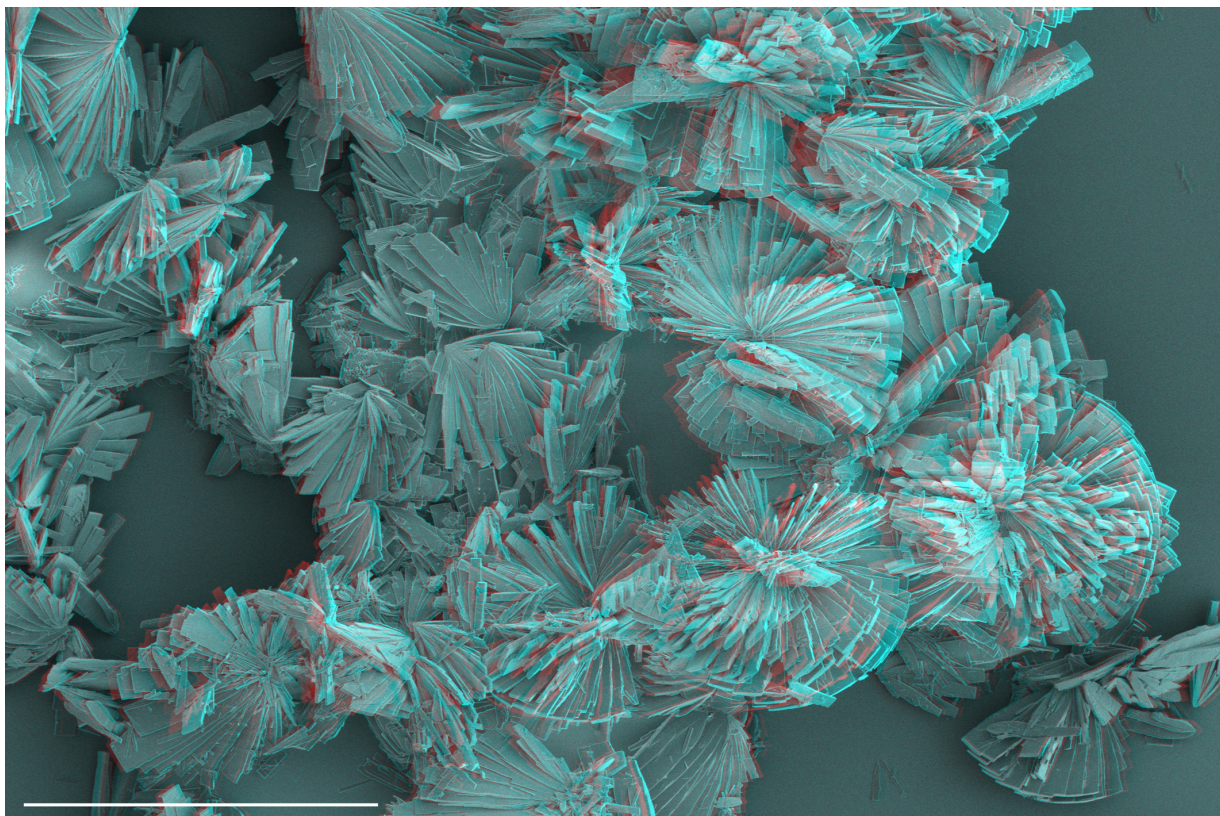
a) SAA14–21 (2.0% w/v) crystallized with acetone vapors at 55 °C - Scale bar: 20 μm



b) SAA14–21 (2.0% w/v) crystallized with acetone vapors at 55 °C - Scale bar: 40 μm



c) SAA14-21 (5.0% w/v) crystallized with liquid acetone at 55 °C - Scale bar: 50 μm .



d) SAA14-21 (5.0% w/v) crystallized with liquid acetone at 55 °C - Scale bar: 40 μm .

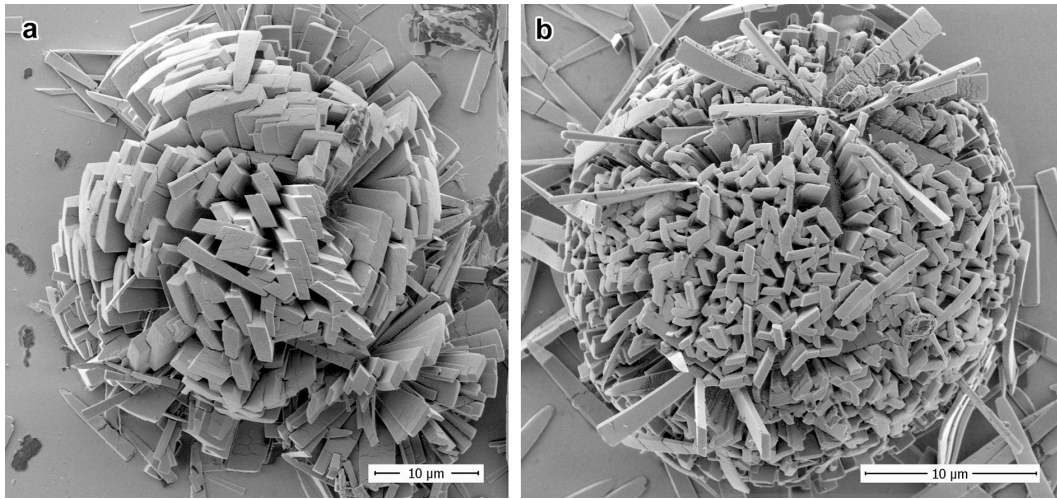


Figure S4. SEM images of assemblies of densely packed A-type amylose crystals prepared from fraction SAA16–22 at 0.05% w/v on a glass slide, by addition of liquid acetone at 55 °C.